COMMUNICATION

On the reconstruction of NiMo electrocatalysts by *operando* spectroscopy

Received 00th January 20xx,
Accepted 00th January 20xx

DOI: 10.1039/x0xx00000x

Jeremy A. Bau,[a] Henrik Haspel,[a] Samy Ould-Chikh,[a] Antonio Aguilar-Tapia,[b] Jean-Louis Hazemann,[b] Hicham Idriss,[c] Kazuhiro Takanabe[a,d]*

Operando **spectroscopy is critical for the understanding of electrocatalytic reactions. The structural dynamics of NiMo, one of the most active non-precious catalysts for H_2 evolution reaction (HER) in alkaline conditions, were studied by X-ray absorption spectroscopy (XAS) and Raman spectroscopy. We observed considerable unexpected results, some of which may change the way we look at data interpretation. During the operando HER conditions under XAS or visible-light laser irradiation, trace amounts of Mo ions were liberated and then redeposited on the electrodes as a Mo^{4+}-containing oxide, giving the appearance that the HER-active catalyst is in the oxide phase. The Mo oxide self-propagated under sufficiently energetic light, resulting in a pattern matching the irradiated catalyst area. Detailed spectroscopic characterization of the role of Mo in NiMo may be hindered under *operando* conditions and care needs to be taken to avoid misleading data interpretation.**

Introduction

In the search for renewable energy vectors, significant attention has been drawn to the generation of H_2 gas through water splitting.[1–3] Electrocatalytic H_2 evolution (HER) is best understood on noble metal catalysts that are impractical for scale-up due to supply constraints. To develop new catalysts with earth-abundant elements for the HER and relevant electrocatalytic reactions, *operando* spectroscopic measurements are critical for understanding active sites and reaction mechanisms on candidate materials because the catalysts are often dynamic under reaction conditions. For example, Mo-based catalysts, particularly NiMo[4,5] represent the best non-noble HER catalysts discovered to date in alkaline conditions. However, Mo stability and dissolution is a common concern, particularly under alkaline conditions that are most realistic for scale-up. While dissolved Mo has been claimed to be associated with improved catalyst activity,[9] its fate in solution is poorly understood.

Dissolved ionic species in other electrocatalytic systems can result in unexpected catalytic activation through unintended deposition on electrodes. For example, trace amounts of dissolved Fe^{3+} are anodically deposited on Ni oxide during the O_2 evolution reaction (OER), resulting in improved catalytic activity.[10–12] Similarly, Co-based OER catalysts dissolve and redeposit under *operando* conditions, conferring long-term stability through self-healing mechanisms.[13] In the case of Co HER catalysts, decomposition of precursor catalysts to metallic Co has been widely demonstrated as the true source of HER activity.[14–16] Electrocatalyst reconstruction can also have negative effects that undermine long-term stability. For example, Cu metal structures are known to undergo dissolution and re-deposition during CO_2 reduction, leading to activity loss.[17–20] Therefore, understanding and controlling such electrochemical phenomena are of both fundamental and practical interest as they provide crucial insights into catalytic mechanisms while determining whether or not a catalyst is truly viable.

In this report, we describe the re-deposition followed by ordered reconstruction of MoO_x from trace concentrations (10 ppm) of Mo formed during *operando* HER under X-ray absorption spectroscopy and visible-light induced Raman analyses of NiMo catalysts. After initial electrochemical deposition, MoO_x catalyzes its continuing photodeposition as long as there is sufficiently energetic irradiation, reductive potentials, and dissolved Mo ions. While the deposited MoO_x does not appear to have any direct effect on the NiMo catalytic activity, it prevented the collection of spectroscopic measurements relevant to the role of Mo in the HER.

[a] *King Abdullah University of Science and Technology (KAUST), KAUST Catalysis Center, Thuwal 23955-6900, Saudi Arabia.*
[b] *Institut Néel, UPR2940 CNRS, University of Grenoble Alpes, F-38000 Grenoble, France.*
[c] *Centre for Research and Development, Saudi Arabian Basic Industries Corporation, KAUST, Saudi Arabia.*
[d] *Department of Chemical Systems Engineering, School of Engineering, The University of Tokyo, 7-3-1 Hongo, Bunkyo-ku, 113-8656, Japan.*
† Electronic Supplementary Information (ESI) available: [Experimental, schema for operando experiments, Supplementary XAS spectra, SEM and AFM images]. See DOI: 10.1039/x0xx00000x

Furthermore, this phenomenon may provide a methodology for the controlled deposition of MoO_x.

Results and discussion

Operando X-ray absorption spectroscopy (XAS) measurement was conducted on NiMo films (bulk Ni:Mo = 4:1) during HER in 0.1 M KOH. Fig. 1 compiles the results of Mo K-edge spectra. Even at low HER rates (−2 mA cm^{-2} at overpotential of ~200 mV, Fig. S2†), NiMo films exhibited a monotonic increase in baseline of Mo X-ray Absorption Near-Edge spectra (XANES) during successive extended X-ray absorption fine structure (EXAFS) scans over the course of 7 h without any sign of deactivation (Fig. 1a). The EXAFS spectrum of the catalyst at the end of the 7-h experiment was dominated by Mo-O bonds (≈ 2.0 Å) and lacked the second-shell Mo-Mo bonds typically seen in ordered Mo oxides, indicating an amorphous oxide (Fig. 1b,c).[21–25] The position of the main edge and the lack of a strong pre-edge structure suggest that the oxidation state of Mo in the catalytically active catalyst was close to Mo^{4+} with an octahedral symmetry,[23–25] counter-intuitively implying that Mo oxidized under cathodic HER-active potentials. In contrast, the freshly deposited alloy exclusively presented a first shell at ~2.5 Å in both the Mo and Ni K-edges corresponding to metal-metal bonds (Fig. 1c, Fig. S3†). Unlike Mo, the Ni signal showed no substantial changes during the acquisition of XAS. Under oxidizing potentials (+0.3 V vs. RHE), the Mo baseline gradually decreased, resulting in the near-restoration of the metallic near-edge structure of the original catalyst over the course of 4 h (Fig. 1d, Fig. S4†). Although these results appeared to contradictorily suggest that Mo oxidation was taking place during reduction (and vice versa), the gradually rising baseline in the Mo spectra implied that the findings were a result of deposition, not oxidation. Confirming this theory, unidimensional scans of the electrode with the synchrotron beam revealed beam-dependent growth of MoO_x at the conclusion of XAS experiments, whereas surrounding regions did not grow at all (spot size 100 µm by 220 µm, Fig. 1e). The height of the growth roughly corresponded to the change in the edge jump during XAS, and the amount of Mo in the spot was 2–4 times greater than the amount of Mo in the surrounding film. Growth was also observed in MoO_x films, demonstrating that the behavior was specific to Mo and took place regardless of the presence of Ni (Fig. 1f).

MoO_x growth and reconstruction on NiMo was also observed in *operando* Raman spectroscopy, demonstrating that the behavior observed in XAS was not an effect related to the interaction of the high flux of X-rays and the electrocatalytic system. With irradiation of a 2-mW laser (λ = 473 nm, spot size 1 $µm^2$), the Raman spectrum of a NiMo electrode was composed of three broad peaks at 270, 500, and 700 cm^{-1}, and one sharp peak at 1000 cm^{-1} at HER (−50 mV vs. RHE) in 0.1 M KOH (Fig. 2a). Changes in the Raman spectrum were commensurate with the appearance of visible spots reflecting the laser illumination size (inset). The sharp peak at ~ 270 cm^{-1} corresponded to the stretching mode of terminal Mo^{6+}=O,[26] whereas the broad peaks at 400-800 cm^{-1} were merged forms of major crystalline MoO_2 Raman peaks[27,28] consistent with the electrodeposited amorphous MoO_x.[29] This result confirms that the deposit is in a Mo^{4+}-containing MoO_2-like amorphous structure. The operando measurements also revealed that the HER performance was not influenced by this MoO_x deposition. Since deposition only affects regions under spot irradiation as opposed to the entire electrode, the effects of the MoO_x on the HER itself are difficult to determine. However, based on the physical similarities with the previously reported material (which was found to be permeable to water),[29] the oxide most likely has no direct effect on the HER.

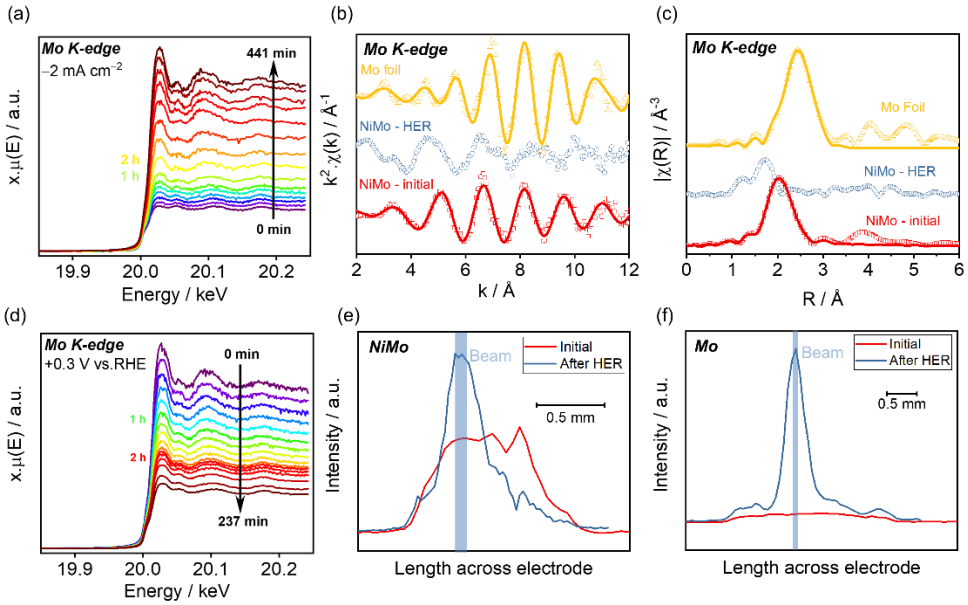

Fig. 1. (a) Operando XANES of Mo K-edge of NiMo at −2 mA cm^{-2}. (b) EXAFS and (c) Fourier transforms of Mo K-edge for NiMo catalyst before (initial) and during HER compared with a spectrum for Mo metal foil. (d) Operando XANES of Mo K-edge of NiMo at 0.3 V vs. RHE after HER in 0.1 M KOH. Mo K-edge line scans of (e) NiMo and (f) Mo (in the absence of Ni) before and after HER experiments (−2 mA cm^{-2}).

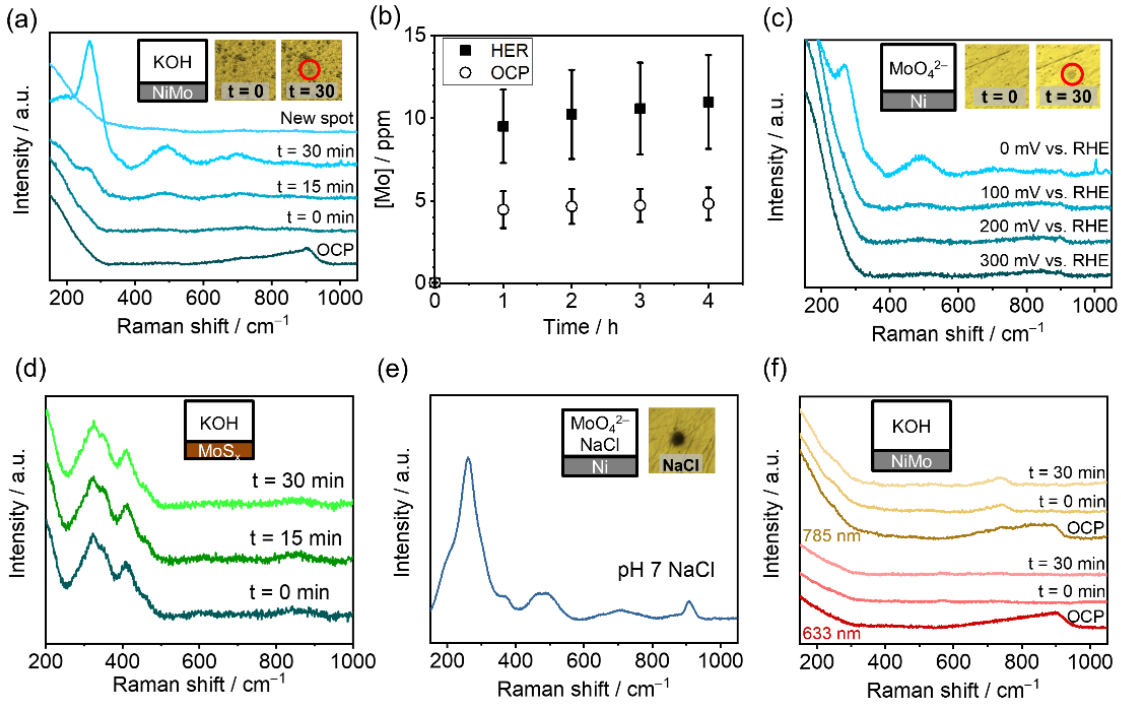

Fig. 2. (a) *Operando* Raman spectra of NiMo catalysts at OCP and 0 V vs. RHE during irradiation with 2-mW/spot 473-nm laser in 0.1 M KOH. (b) Concentration of dissolved Mo determined by ICP-MS of NiMo films in small volumes (5 mL) of 0.1 M KOH under HER (−2 mA cm^{-2}) and open circuit potential (OCP) conditions. Error bars achieved by repeating experiments four times. (c) Raman spectra collected using 2-mW/spot 473-nm laser at different potentials in 1 mM Na_2MoO_4/0.1 M KOH on Ni electrode. (d) *Operando* Raman spectra of cathodically electrodeposited MoS_x films collected using 2-mW/spot 473-nm laser at 0 V vs. RHE in 0.1 M KOH. (e) *Operando* Raman spectra collected using 2-mW/spot 473-nm laser at 0 V vs. RHE in 1 mM Na_2MoO_4/0.5 M NaCl (pH 7) on Ni. (f) *Operando* Raman spectra of NiMo catalyst at OCP and 0 V vs. RHE during irradiation with 2-mW/spot 633 and 785-nm lasers in 0.1 M KOH. Inset images in (a) and (c) depict the irradiated area before and after 30 min irradiation. Inset image in (e) was the result of 30 min irradiation.

Formation and stability of MoO_x in highly alkaline conditions are not predicted by the electrochemical equilibrium of Mo in aqueous solutions,[30,31] but indeed non negligible amounts of dissolved Mo (~10 ppm, ~ 0.1 mM) were detected in the electrolyte upon cathodic application compared to NiMo catalyst left at open circuit potential (OCP) (Fig. 2b). Nonetheless, deposition can be repeated on a Mo-free electrode in an electrolyte with trace Mo using otherwise similar conditions (0.1 M KOH/1 mM Na_2MoO_4, potentials at and more cathodic than 0 V vs. RHE) (Fig 2c). According to both the Pourbaix diagram for Mo and prior knowledge of Mo oxides in aqueous conditions, Mo undergoes a series of redox events (3+/6+, 3+/4+, 4+/6+) near 0 V vs. RHE.[30–32] Since Na_2MoO_4 solutions do not absorb visible light (Fig. 3a), we propose that a layer of MoO_x is first electrodeposited onto the electrode surface, which in turn propagates in the presence of both light and cathodic potential. The photodeposition effect did not take place with amorphous MoS_x, another Mo-based HER catalyst with good HER activity and stability particularly in acidic condition (Fig. 2d).[6] Deposition also took place at less caustic conditions (pH 7, 0.5 M NaCl), making this phenomenon amenable for depositing MoO_x features (Fig. 2e).

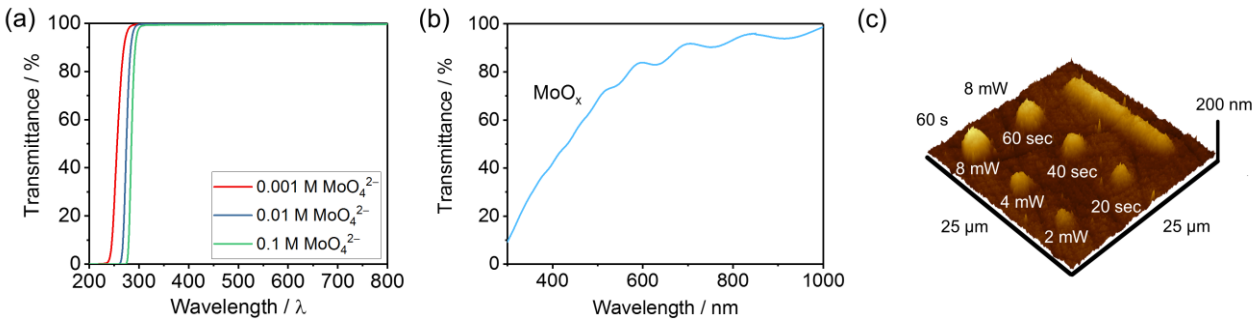

Fig. 3. (a) UV-vis spectra of different concentrations of Na_2MoO_4 solutions, (b) UV-vis spectrum of MoO_x film deposited on FTO at −0.4 V vs. RHE and 300 W of Xe irradiation, normalized to the UV-vis spectrum of blank FTO. (c) AFM profile of MoO_x photolithographic patterns. Effects of irradiation power for 1 min (8, 4, 2 mW, left to right, bottom left row) and varying irradiation time at 8 mW (60, 40, 20 s, left to right, middle row).

In contrast to the behavior under 473 nm laser irradiation, NiMo electrodes irradiated at higher wavelengths (λ = 633, 785 nm) did not exhibit MoO_x growth (Fig. 2f), suggesting that photoexcitation is bandgap-like origin. To examine the optical properties of MoO_x, large surface area MoO_x films were deposited on transparent fluorine-doped tin oxide (FTO) electrodes from 0.1 M KOH/0.1 M Na_2MoO_4 using a 300-W Xe lamp and a cold mirror (λ < 450 nm) at −0.4 V vs. RHE. The broad absorption of the MoO_x films in a wide range of visible light is consistent with the previously determined absorption characteristics for semiconducting MoO_2, with a bandgap close to 2.5 eV (corresponding to a wavelength ~500 nm) that explains the ability of MoO_x to absorb 473 nm but not 633 nm irradiation (Fig. 3b).[33,34] A weak but non-negligible photo-response was detected by such MoO_x films under illumination (Fig. S5†). The successful deposition on FTO has thus confirmed that the substrate nature had no effect on the deposition phenomenon. A thermal cause for deposition was excluded due to the lack of MoO_x growth under infrared light (785 nm), as well as the increased MoO_x dissolution at higher temperatures.[35]

Based on the behavior of MoO_x films arising from dissolved Mo, we propose the following mechanism of MoO_x deposition on NiMo and subsequent behavior under irradiation (Scheme 1). Initially, under cathodic potentials, hydroxides are generated. Subsequently, a small fraction of Mo dissolves into the electrolyte solution (as Mo^{6+}), due to local increases in pH. Finally, Mo^{6+} is redeposited on the surface of the NiMo as an initial layer of MoO_x that grows upon further absorption of radiation of sufficient energy, resulting in the reduction of dissolved Mo^{6+} to a Mo^{4+}-containing oxide by excited electrons transferred from the CB of MoO_2. Meanwhile, dissolution gradually takes place under OCP due to the high pH, but is accelerated at 0.3 V vs. RHE due to the application of anodic current. Using these simple steps, we provide a proof-of-concept technique for depositing MoO_x nanostructures using a confocal Raman setup in 1 mM Na_2MoO_4/0.5 M NaCl at 0 V vs. RHE with a 473-nm laser (Fig. 3c). Modulating the intensity of the incident laser on the substrate (2–8 mW) and the exposure time (20–60 s) yielded features with thicknesses of 50–150 nm (Figs. S6, S7†). Furthermore, more complicated patterns such as lines can be prepared by repeated scanning (Fig. 3c). This well-controlled deposition technique may be applicable to advanced electrode and photoelectrode fabrication for active and durable HER performance.

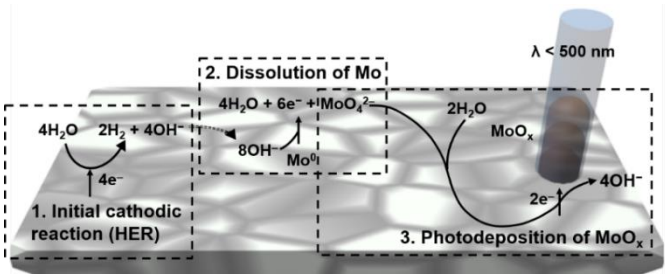

Scheme 1. Proposed mechanism of Mo dissolution and re-deposition under irradiation on NiMo electrocatalyst electrodes.

Conclusions

Photon-induced deposition of amorphous MoO_x from dissolved Mo cations in *operando* study of NiMo HER has been observed. This deposition did not affect the HER activity but altered the Mo-K edge spectra significantly in a manner that may induce erroneous conclusions related to redox reactions. The ability of the photoelectrochemical reaction to counter the alkaline dissolution of Mo ions is also potentially useful for depositing conformal MoO_x patterns without the need for an overly complicated setup. A multiple-step mechanism involving dissolution, deposition and light stimulated growth of MoO_x (x ~ 2) was proposed. Ultimately, NiMo remains the top-performing non-precious alkaline HER catalyst, but the reconstruction of Mo limits potential characterization approaches.

Conflicts of interest

There are no conflicts to declare.

Acknowledgements

The research reported in this study was supported by the King Abdullah University of Science and Technology. The authors acknowledge the support of SABIC in funding this research. The FAME-UHD project is financially supported by the French large loan EquipEx (EcoX, ANR-10-EQPX-27-01), the CEA-CNRS CRG consortium and the INSU CNRS Institute.

Notes and references

1 J. H. Montoya, L. C. Seitz, P. Chakthranont, A. Vojvodic, T. F. Jaramillo, J. K. Nørskov, Nat. Mater. 2017, **16**, 70–81.
2 M. Zeng, Y. Li, J. Mater. Chem. A, 2015, **3**, 14942.
3 X. Li, X. Hao, A. Abudula, G. Guan, J. Mater. Chem. A, 2016, **4**, 11973.
4 J. Zhang, T. Wang, P. Liu, Z. Liao, S. Liu, X. Zhuang, M. Chen, E. Zschech, X. Feng, Nat. Commun. 2017, **8**, 15437.
5 P. M. Csernica, J. R. McKone, C. R. Mulzer, W. R. Dichtel, H. D. Abruña, F. J. DiSalvo, ACS Catal., 2017, **7**, 3375.
6 P. D. Tran, T. V. Tran, M. Orio, S. Torelli, Q. D. Truong, K. Nayuki, Y. Sasaki, S. Y. Chiam, R. Yi, I. Honma, et al., Nat. Mater. 2016, **15**, 640–646.
7 Y. Ouyang, Q. Li, L. Shi, C. Ling, J. Wang, J. Mater. Chem. A 2018, **6**, 2289.
8 I. Roger, R. Moca, H. N. Miras, K. G. Crawford, D. A. J. Moran, A. Y. Ganin, M. D. Symes, J. Mater. Chem. A, 2017, **5**, 1472.
9 C. Lupi, A. Dell'Era, M. Pasquali, Int. J. Hydrogen Energy 2014, **39**, 1932.
10 L. Trotochaud, S. L. Young, J. K. Ranney, S. W. Boettcher, J. Am. Chem. Soc., 2014, **136**, 6744.
11 M. P. Browne, S. Stafford, M. O'Brien, H. Nolan, N. C. Berner, G. S. Duesberg, P. E. Colavita, M. E. G. Lyons, J. Mater. Chem. A, 2016, **4**, 11397.
12 Y. Kuang, Q. Jia, G. Ma, T. Hisatomi, T. Minegishi, H. Nishiyama, M. Nakabayashi, N. Shibata, T. Yamada, A. Kudo, et al., Nat. Energy, 2017, **2**, 16191.
13 D. A. Lutterman, Y. Surendranath, D. G. Nocera, J. Am. Chem. Soc., 2009, **131**, 3838.

14 N. Kaeffer, A. Morozan, J. Fize, E. Martinez, L. Guetaz, V. Artero, ACS Catal., 2016, **6**, 3727.
15 B. Lassalle-Kaiser, D. Merki, H. Vrubel, S. Gul, V. K. Yachandra, X. Hu, J. Yano, J. Am. Chem. Soc., 2015, **137**, 314.
16 Y. Zhu, H.-C. Chen, C.-S. Hsu, T.-S. Lin, C.-J. Chang, S.-C. Chang, L.-D. Tsai, H. M. Chen, ACS Energy Lett., 2019, **4**, 987.
17 J. Huang, N. Hörmann, E. Oveisi, A. Loiudice, G. L. D. Gregorio, O. Andreussi, N. Marzari, R. Buonsanti, Nat. Commun. 2018, **9**, 3117.
18 P. D. Luna, R. Quintero-Bermudez, C.-T. Dinh, M. B. Ross, O. S. Bushuyev, P. Todorović, T. Regier, S. O. Kelley, P. Yang, E. H. Sargent, Nat. Catal., 2018, **1**, 103.
19 J. He, A. Huang, N. J. J. Johnson, K. E. Dettelbach, D. M. Weekes, Y. Cao, C. P. Berlinguette, Inorg. Chem. 2018, **57**, 14624.
20 Z. Weng, X. Zhang, Y. Wu, S. Huo, J. Jiang, W. Liu, G. He, Y. Liang, H. Wang, Angew. Chem. Int. Ed. 2017, **56**, 13135.
21 H. Shimada, N. Matsubayashi, T. Sato, Y. Yoshimura, A. Nishijima, N. Kosugi, H. Kuroda, J. Catal., 1992, **138**, 746.
22 O. Hirsch, G. Zeng, L. Luo, M. Staniuk, P. M. Abdala, W. van Beek, F. Rechberger, M. J. Süess, M. Niederberger, D. Koziej, Chem. Mater. 2014, **26**, 4505.
23 T. Ressler, O. Timpe, T. Neisius, J. Find, G. Mestl, M. Dieterle, R. Schlögl, J. Catal. 2000, **191**, 75.
24 T. Ressler, J. Wienold, R. E. Jentoft, T. Neisius, J. Catal. 2002, **210**, 67.
25 Y. Zhou, H. Xie, C. Wang, Q. He, Q. Liu, Z. Muhammad, Y. A. Haleem, Y. Sang, S. Chen, L. Song, J. Phys. Chem. C 2017, **121**, 15589.
26 W. Liu, Q. Xu, W. Cui, C. Zhu, Y. Qi, Angew. Chem. Int. Ed. 2017, **56**, 1600.
27 Y. Jin, P. K. Shen, J. Mater. Chem. A, 2015, **3**, 20080.
28 X. Xia, S. Deng, D. Xie, Y. Wang, S. Feng, J. Wu, J. Tu, J. Mater. Chem. A, 2018, **6**, 15546.
29 A. T. Garcia-Esparza, T. Shinagawa, S. Ould-Chikh, M. Qureshi, X. Peng, N. Wei, D. H. Anjum, A. Clo, T.-C. Weng, D. Nordlund, et al. Angew. Chem. Int. Ed. 2017, **56**, 5780.
30 V. S. Saji, C.-W. Lee, ChemSusChem, 2012, **5**, 1146.
31 M. Pourbaix, Atlas of Electrochemical Equilibria in Aqueous Solutions; Pergamon Press: New York, 1966.
32 K. Machida, M. Enyo, J. Electrochem. Soc. 1990, **137**, 1169.
33 K. Inzani, M. Nematollahi, F. Vullum-Bruer, T. Grande, T. W. Reenaas, S. M. Selbach, Phys. Chem. Chem. Phys. 2017, **19**, 9232.
34 N. Dukštienė, D. Sinkevičiūtė, J Solid State Electrochem., 2013, **17**, 1175.
35 J. B. Lee, Corrosion, 1981, **37**, 467–481.